1-1-2011

Numerical Modelling of Interrogation Systems for Optical Fibre Bragg Grating Sensors

Daniel P. Oswald
Edith Cowan University

Steven J. Richardson
Edith Cowan University

Graham Wild
Edith Cowan University

10.1117/12.903544

Numerical Modelling of Interrogation Systems for Optical Fibre Bragg Grating Sensors

Daniel Oswald[a], Steven Richardson[b], Graham Wild*[a]
[a]Photonics Research Lab., Edith Cowan Univ., 270 Joondalup Dr., Joondalup, WA Australia 6027;
[b]School of Engineering, Edith Cowan Univ., 270 Joondalup Dr., Joondalup, WA Australia 6027

ABSTRACT

There are a number of interrogation methods that can be used in optical Fibre Bragg Grating (FBG) sensing system. For very high frequency signals interrogating the sensor signal from an FBG is limited to two intensiometric methods, edge filter detection and power detection. In edge filter detection, a broadband light source illuminates an FBG, the reflected spectrum is then passed through a spectral filter. In power detection, a narrowband light source with a wavelength corresponding to the 3dB point of the FBG is filtered by the FBG itself. Both methods convert the spectral shift of the FBG into intensity signals. These two categories each have a number of variations, all with different performance characteristics. In this work we present a numerical model for all of these interrogation systems. The numerical model is based on previous analytical modelling, which could only be utilised for perfect Gaussian profiles. However, interrogation systems can make use of non Gaussian shaped filters, or sources. The numerical modelling enables the different variations to be compared using identical component performance, showing the relative strengths and weakness of the systems in terms of useful parameters, including, signal-to-noise ratio, sensitivity, and dynamic resolution. The two different detection methods can also be compared side-by-side using the same FBG. Since the model is numerical, it enables real spectral data to be used for the various components (FBG, light source, filters). This has the added advantage of increasing the accuracy and usefulness of the model, over previous analytical work.

Keywords: Analytical modelling, fibre Bragg gratings, interrogation systems, numerical modelling, optical fibre sensing

1. INTRODUCTION

Fibre Bragg Grating (FBG) sensors were first reported by Morey, Meltz and Glenn [1], in 1989, following their transverse holographic fabrication method for FBGs [2]. Typically, FBG sensing applications tend to focus on the use of FBGs as spectral sensing elements. That is, the measurand signal is encoded into the wavelength of the FBG. The absolute nature of spectrally encoding makes FBG sensors immune to issues such as optical power fluctuations. It also enables large numbers of FBGs to be multiplexed along lengths of optical fibre. The spectral property of FBGs means they can be easily multiplexed using Wavelength Division Multiplexing (WDM) [3]. As optical fibre sensors, FBGs have several other properties that make them of interest to sensing [4]. The most significant of these advantages include reduced size and weight, immunity to electromagnetic interference, and most significantly, the versatility of FBGs to detect different measurands. An FBG sensor can be used to detect both static and dynamic signals. Static signals include temperature, pressure, and static strain, while dynamic signals include acoustic emissions, actively generated acousto-ultrasonic signals, and dynamic strain (e.g. vibration).

However, there are disadvantages associated with spectrally encoding the sensing signal. Specifically, the required spectral decoding of the sensor signals is slow, expensive, and processor intensive. Alternatively, FBGs can be used as intensity based sensors. That is, the change in the spectral information of the FBG from the applied measurand can easily be converted into an intensity change, using either edge filter detection or power detection [5]. The use of an intensity based systems means that problems such as input optical power fluctuations can be reintroduced into the system. However, the advantages of edge filter detection, specifically the speed and simplicity of detection, greatly outweigh the corresponding disadvantages.

* G.Wild@ecu.edu.au; phone 61 8 6304 5780; fax 61 8 6304 5811; se.ecu.edu.au

Smart Nano-Micro Materials and Devices, edited by Saulius Juodkazis, Min Gu, Proc. of SPIE
Vol. 8204, 82040Q · © 2011 SPIE · CCC code: 0277-786X/11/$18 · doi: 10.1117/12.903544

For example, commercial interrogators are available for FBG sensing. The si920 interrogator is capable of 100kHz acquisition on four channels (Micron Optics, Atlanta, GA), and the SFI710 interrogator is capable of 40kHz acquisition on eight channels (Fiberpro, San Jose, CA). These interrogation systems are typically used for quasi-static measurands, such as temperature and strain. However, for very high frequency dynamic signals, such as acoustic emissions, or ultrasound in general, these commercial interrogation systems cannot be used. Instead, an intensity based interrogation method must be utilised.

In an effort to compare the efficiency of different intensity based interrogation an analytical model was initially developed [6]. This model simulated a simple power detection based intensiometric interrogation system. The approach implemented was similar to that of Nunes et al. [7]. However, this method was simplified by assuming that the laser and FBG could be expressed as basic Gaussian functions. As a result, an analytical model could be used since the multiplication of Gaussians functions results in a Gaussian, and their integrals are well understood. However, when involving components that do not have a Gaussian spectral response, an analytical solution may not be defined; hence truly numerical methods are required. In this work, we present results from different numerical techniques to compare with the analytical results previously reported [6]. With the successful implementation of a numerical method, we model the performance of edge filter based intensiometric interrogation systems. As with the analytical model, the numerical model is capable of time dependent measurements, which enables high frequency dynamic AC signal to be modelled. The models are implemented in MATLAB (Math Works, Natwick, MA).

2. BACKGROUND

2.1 Fibre Bragg Gratings

A FBG [8] is a spectrally reflective element written into the core of an optical fibre. The FBG is made up of alternating regions of different refractive indices. The difference in refractive indices results in Fresnel reflection at each interface. The regular period of the grating, Λ, results in constructive interference in the reflection at a specific wavelength, called the Bragg wavelength, λ_B. The Bragg wavelength is given as,

$$\lambda_B = 2n\Lambda\,, \tag{1}$$

where n is the average refractive index of the grating.

Equation (1) indicates that any measurand that causes either a change in the refractive index or grating period can be detected with the FBG. For measuring acoustic and ultrasonic signals, the measurand is applied strain. A change in grating period is a direct result of the applied strain, while the change in refractive is a result of the strain-optic effect. Ignoring the temperature effect, the relative change in the Bragg wavelength ($\Delta\lambda_B$) as a function of the applied strain (ε) or a change in Temperature (ΔT) can then be expressed as,

$$\Delta\lambda_B = \lambda_B\left[\varepsilon\left(1-\frac{n^2}{2}\left[p_{12}-\nu\left(p_{12}+p_{11}\right)\right]\right)+\Delta T\left(\alpha+\frac{1}{n}\frac{dn}{dT}\right)\right], \tag{2}$$

where ν is Poisons' ratio, p_{12} and p_{11} are the strain optic coefficients, α is the thermooptic coefficient, an dn/dT is the rate of change of the refractive index with the changing temperature. Equation (2) then enables the strain applied to the grating, or the temperature change, to be converted into the shift in the wavelength which can be easily determined via an interrogator.

2.2 Interrogation Methods

There are two broad interrogation methods available for the detection of high frequency acoustic signal with FBGs. These are edge filter detection methods, and power detection methods [5]. A small number of active detection methods are available, such as pseudo-heterodyning, but these are not considered in this review, as their implementation is small in comparison to the passive methods used.

2.2.1 Edge Filter Detection Methods

In edge filter detection methods, the shift in the FBG spectrum is detected by use of a spectrally-dependent filter which results in a change in intensity at the detector. The FBG is illuminated by a broadband source, such as a SLD. The change in the wavelength reflected causes the transmitted intensity to vary as the filters transmittance varies as a function of wavelength. A number of different filters can be utilised, including a matched FBG [9], a linear edge absorption filter, an interference filter [10], a Wavelength Division Multiplexing (WDM) coupler [11], an Arrayed Wave Guide (AWG) [12], and a Dense Wavelength Division Multiplexing (DWDM) filter.

The most straight-forward edge filter detection methods is the linear edge absorption filter. Typically an external filter is used. The FBG is selected such that the Bragg wavelength is at the 3dB point of the absorption filters transmittance. The light not transmitted to the detector is absorbed by the filter.

A improvement on the use of a linear edge absorption filter is the WDM coupler. This is a three port device, where the input is split between two outputs depending on the wavelength. The spectral response of the WDM coupler is such that a linear edge occurs between the wavelength of the first output and the second output. In operation, the WDM coupler works exactly the same as the linear edge absorption filter, except now the light which is not transmitted to the output is not absorbed; it is directed to the second output. This can be used to give a differential output.

The simplest edge filter is a matched FBG. Here an identical FBG is used as the filter which converts the spectral shift of the FBG into an intensity change. If there is no change in measurand, the reflected wavelength from the sensing FBG will match the Bragg wavelength of the filter FBG, and hence no light will be transmitted to the detector. As the wavelength of the sensing FBG shifts, the intensity transmitted by the unshifted filtering FBG will increase. The only drawback to this system is that the nature of the strain (tensile or compressive) cannot be determined directly due to the symmetric nature of the curves. Also, frequency doubling will occur due to this fact since the acoustic wave is both tensile and compressive. To overcome this, the matched FBG is not identical, but typically has a linear edge, and the Bragg wavelength of the sensing FBG is matched to the 3dB point of the linear edge.

The final two edge filter detection methods, AWG and DWDM filter, are identical in their implementations. Both the AWG and DWDM filter are multichannel devices. The edges of the devices are too steep to use directly, however the channels are spaced close enough together such that the signal will cause a differential variation in neighbouring channels, if the FBG is such that its Bragg wavelength is located between the two neighbouring channels. Figure 1 shows various optical circuits corresponding to the different edge filter detection methods.

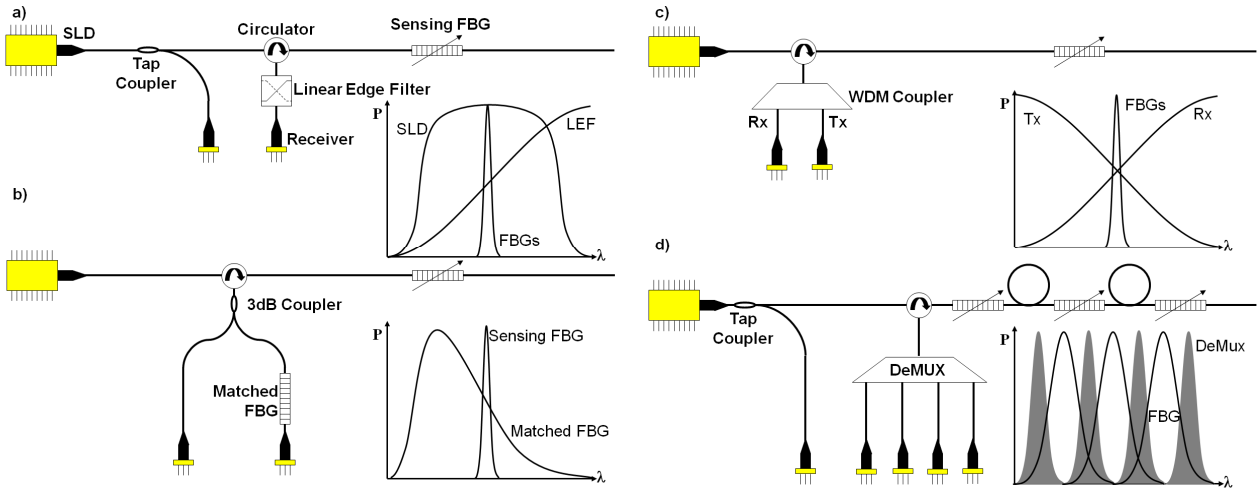

Figure 1. Optical circuits of the edge filter detection methods using a broadband (SLD) source, a) linear edge filter (LEF), b) matched FBG, c) WDM coupler, and d) AWG or DWDM DeMUX incorporating multiplexing. Insets show spectra of the optical components.

2.2.2 Power Detection Methods

In power detection methods, the shift in the FBG wavelength is detected by using a spectrally-dependent source, which results in a change of intensity at the detector as the sensing FBG shifts due to the applied signal. There are two power detection methods, linear edge source [5], and the narrow bandwidth source [13].

In the linear edge source power detection, the edge of a relatively broadband source (source bandwidth > FBG bandwidth) is used, and the FBG is chosen such that the Bragg wavelength is located at the 3dB point of the source. The wavelength shift of the FBG will then result in a direct change in the reflected intensity as it shifts up and down the edge of the source's spectrum.

The second power detection method is the opposite of the linear edge source, such that a relatively narrow bandwidth source (source bandwidth < FBG bandwidth) is set to the 3dB point of the FBG. Here, either the reflected power can be utilized [13], or the transmitted power can be utilized [14], individually, or together in Transmit Reflect Detection (TRD) [15]. Figure 2 shows the optical circuits of the various power detection methods.

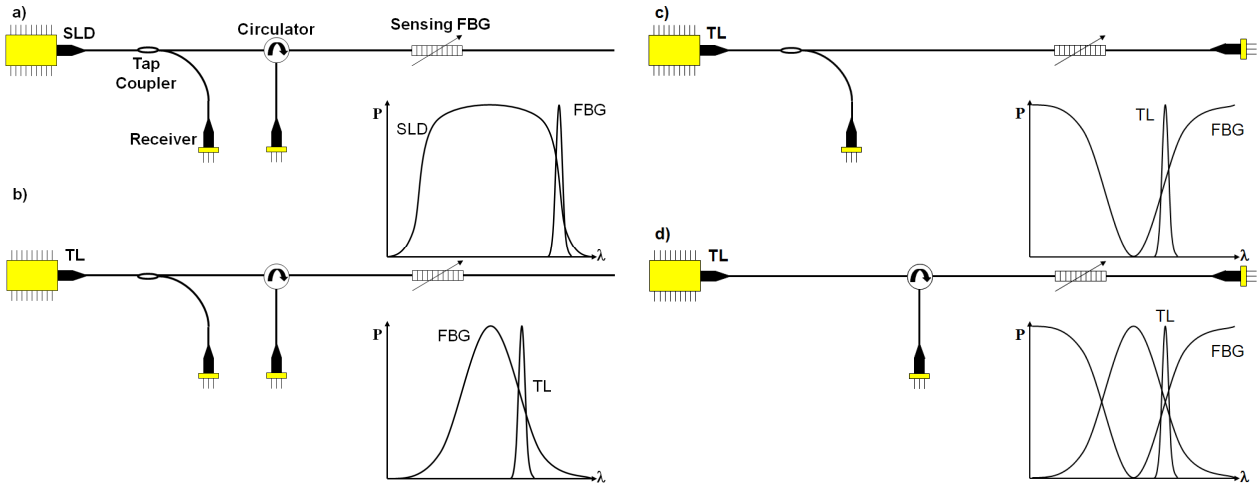

Figure 2. Optical circuits of the power detection methods, a) broadband source (SLD) power detection, and narrow bandwidth source using b) the reflected component, c) the transmitted component, and d) both the transmitted and reflected components together. Insets show spectra of the optical components.

3. THEORY

3.1 Analytical Model

3.1.1 Power Detection

Since the spectral output of the laser is assumed to be a Gaussian, it can be expressed as,

$$L(\lambda) = L_0 \exp\left[-\alpha_L (\lambda - \lambda_L)^2\right]. \tag{3}$$

Here, λ_L is the centre wavelength of the laser, α_L is the width of the Gaussian, and L_0 is the amplitude of the Gaussian. The width of a Gaussian is related to the linewidth ($\Delta\lambda$) or FWHM by,

$$\alpha = \frac{\ln 16}{(\Delta\lambda)^2}. \tag{4}$$

The amplitude of the Gaussian that describes the laser (L_0) is related to the total optical power (P) emitted by the laser by the relationship,

$$L_0 = P\sqrt{\frac{\alpha_L}{\pi}}\ . \tag{5}$$

The spectral response of the FBG can also be expressed as a Gaussian. That is,

$$S(\lambda) = S_0 \exp\left[-\alpha_S(\lambda - \lambda_S)^2\right], \tag{6}$$

where λ_S is the Bragg wavelength, and S_0 is the peak reflectivity of the FBG, which will typically have a value of one for a single FBG sensors (as in this model), or for FBGs used in wavelength division multiplexing.

The portion of the laser power that is reflected (R) by the FBG as a function of wavelength is given as,

$$R = \int_{-\infty}^{\infty} LSd\lambda\ . \tag{7}$$

The component of the laser power transmitted (T) as a function of wavelength is given by, the total laser spectrum, subtract the reflected component. That is,

$$T = \int_{-\infty}^{\infty} Ld\lambda - \int_{-\infty}^{\infty} LSd\lambda = P - R\ . \tag{8}$$

Equation (7) contains two Gaussians multiplied together. The result of this is another Gaussian centred between them. This then gives an analytical solution to (7) which is,

$$R = S_0 L_0 \sqrt{\frac{\pi}{\alpha_S + \alpha_L}} \exp\left[-\frac{\alpha_S \alpha_L}{\alpha_S + \alpha_L}(\lambda_S - \lambda_L)^2\right]. \tag{9}$$

3.1.2 Edge Filter Detection

In edge filter detection, the laser function (3) becomes the LED function. The difference being that the LED will have a much broader emission spectrum. In addition to this, a filter function needs to be incorporated, which can have a variety of spectral response, depending on the type selected (see Section 2.2.1). For example, an ideal linear edge filter with a positive slope would have the form,

$$F = \begin{cases} 0 & \lambda < \lambda_0 \\ \dfrac{1}{\Delta\lambda_F}(\lambda - \lambda_0) & \lambda_0 \le \lambda \le (\lambda_0 + \Delta\lambda_F), \\ 1 & \lambda > (\lambda_0 + \Delta\lambda_F) \end{cases} \tag{10}$$

where λ_0 is the lower edge of the linear edge, and $\Delta\lambda_F$ is the span of the linear edge of the filter.

The only change that needs to be made to (7) is the multiplication of the reflected signal with this filter, giving,

$$R = \int_{-\infty}^{\infty} LSFd\lambda\ . \tag{11}$$

For the edge filter detection method, the transmitted component can be omitted.

3.2 Numerical Method

Three different numerical techniques were used to evaluate the integral in (7) or (11). These techniques are the midpoint rule, the trapezoid rule, and Simpson's rule.

3.2.1 Midpoint Rule

The midpoint rule, also known as the rectangle method, uses a series of rectangles and computes an approximation to a definite integral. The height of the rectangles is determined by the values of the function at midpoint of the rectangle.

That is, over a discrete interval, the function being integrated is replaced by a series of constants, and the area under the constants is used to approximate the area of the original function. This is shown in Figure 3.

Let $x_i = a + ih$ for $i = 0, 1, \ldots, n$ with $h = (b-a)/n$. The mid-point rule formula is given by [16],

$$\int_a^b f(x)dx \approx h\sum_{i=0}^{n-1} f\left(\frac{x_i + x_{i+1}}{2}\right). \tag{12}$$

3.2.2 Trapezoid Rule

The second approximation that was used is the trapezoid rule. In contrast to the mid-point rule trapezoids are used to approximate the area under the curve instead of rectangles. That is, over a discrete interval, the function being integrated is replaced by a series of linear function, and the area under the linear functions is used to approximate the area of the original function. This is shown in Figure 3.

Let $x_i = a + ih$ for $i = 0, 1, \ldots, n$ with $h = (b-a)/n$. The trapezoid rule formula is given by [16],

$$\int_a^b f(x)dx \approx \frac{h}{2}\left[f(x_0) + \sum_{i=1}^{n-1} f(x_i) + f(x_n)\right].$$

3.2.3 Simpson's Rule

Simpson's rule uses a locally parabolic approximation to the integrand function instead of the straight line segments used in the previous methods. That is, over a discrete interval, the function being integrated is replaced by a quadratic function, and the area under the quadratic function is used to approximate the area of the original function. This is shown in Figure 3.

Let $x_i = a + ih$ for $i = 0, 1, \ldots, n$ with $h = (b-a)/n$. The Simpson's rule formula is given by [16],

$$\int_a^b f(x)dx \approx \frac{h}{3}\left[f(x_0) + 2\sum_{i=1}^{n/2-1} f(x_{2i}) + 4\sum_{i=1}^{n/2} f(x_{2i-1}) + f(x_n)\right].$$

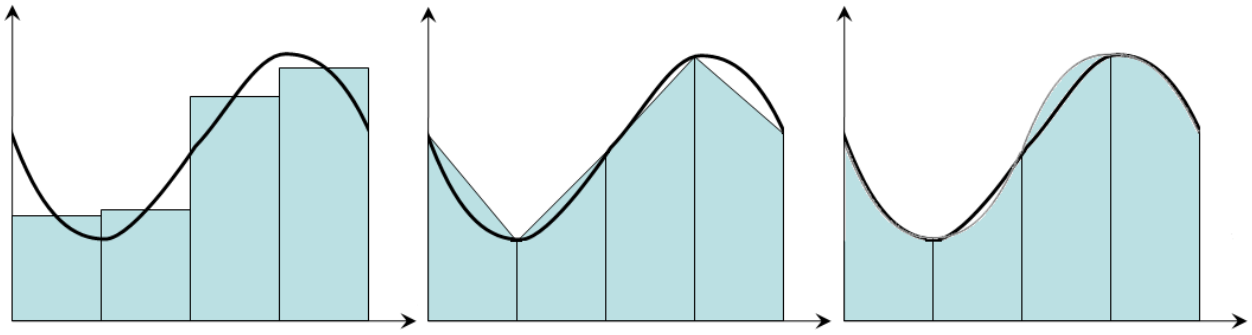

Figure 3. From left to right, the improvement of the numerical approximation, from the Mid Point Rule, through the Trapezoid Rule, to Simpson's Rule.

4. RESULTS

4.1 Numerical Method Comparison

First the three different numerical techniques were compared to determine which the best method to implement was. Here the numerical methods were compared to the equivalent analytical solution. This involved a power detection

interrogation system, using a laser with a bandwidth of 0.082nm, with an optical power of 10mW, and a FBG with a bandwidth of 0.8nm, with a reflectivity of 1, and a Bragg wavelength of 1553.73nm. These specifications are similar to those used experimentally [17].

A static comparison was performed to compare the three numerical integration methods. Here the laser wavelength was swept from 1553.13nm to 1554.13nm, in 1pm increments. The 2nm region of the integration from (7), at every laser wavelength, was divided into three different subregions, 100 points, 1000 points, and 10000 points.

Figure 4 shows the results from the numerical integration comparison. In Figure 4 a) we see there is little difference between the analytical solution and the three numerical methods. As a result, differences were taken between the analytical and numerical solutions, shown in Figure 4 b) to d). As the number of integration points increases, the size of the error using Simpson's rule decreases. However, the other two integration methods showed a more complex relationship as the number of integration points increased. That is, there is an oscillation in the error, which is understandable, as the rectangles or trapezoids over estimate, then underestimate the area under the Gaussian. However, over 100 integration points, the error associated with both of these methods is still insignificant.

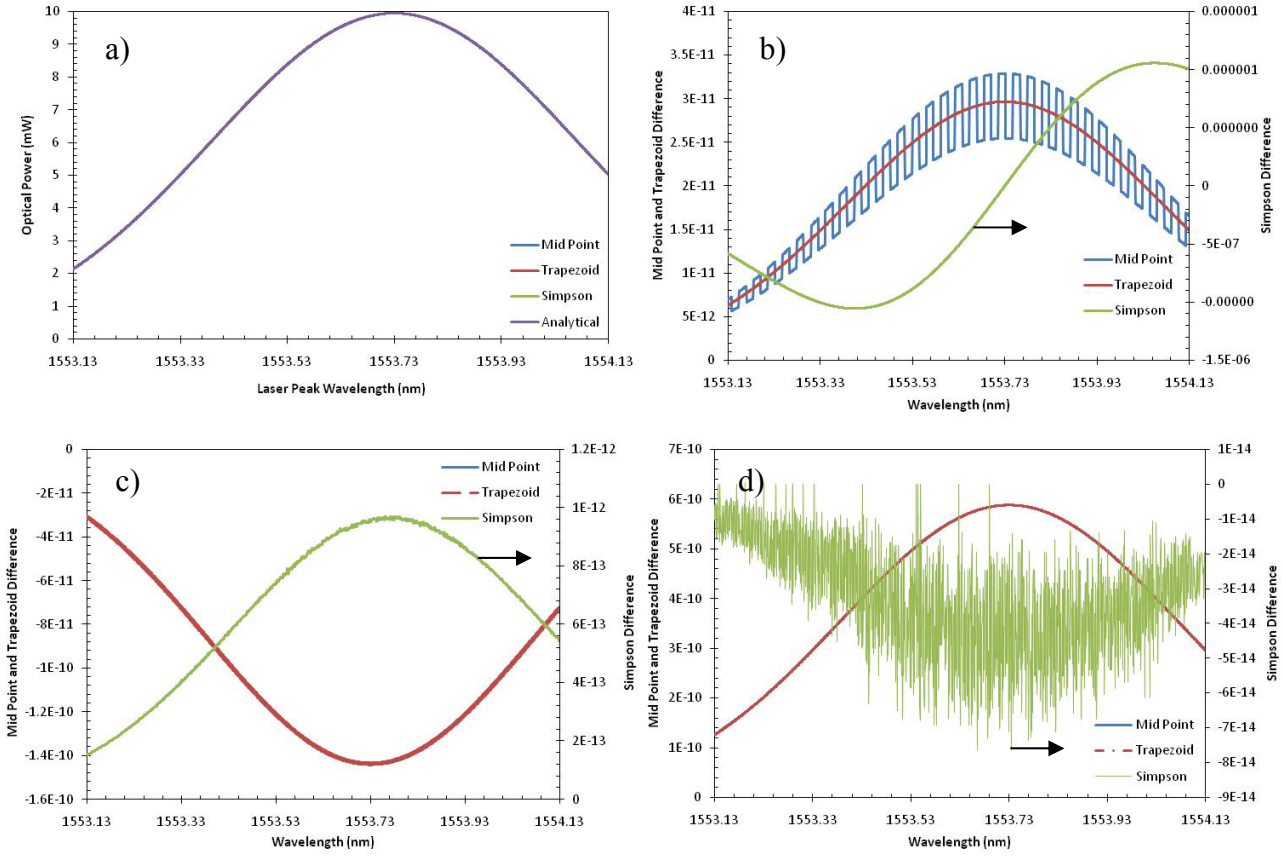

Figure 4. a) Optical power reflected from the FBG as the laser wavelength is swept across it, evaluating (7) analytically, and with the three numerical methods, with 100 integration points per wavelength. Difference between the three numerical methods and the analytical solution for, b) 100 integration points, c) 1000 integration points, and d) 10000 integration points/

The result of the numerical technique comparison showed that the exact choice of the three numerical methods showed little impact on the result, given the small size of the differences, or errors. As a result, the implementation for further work only used the trapezoid rule, with 1000 integration points. The reason for this was partly due to consistent regular difference (error), but also the simple implementation in code, reducing simulation times. However, the most important

reason was that the trapezoid rule works perfectly for discrete data. This is ideal for real experimental spectral data collected from an optical spectrum analyser. In contrast the standard midpoint rule, would need to evaluate integration points between every data point, using a linear approximation.

4.2 Power Detection Methods

Following the selection of the trapezoid rule for the numerical integration, the numerical model was expanded to incorporate all three power detection interrogation methods, reflection, transmission, and TRD. As before, the numerical solution of the model agreed significantly with the analytical solution. Figure 5 shows no detectable difference between the numerical and analytical solutions, using the 1000 integration points, as the laser was swept across the FBG.

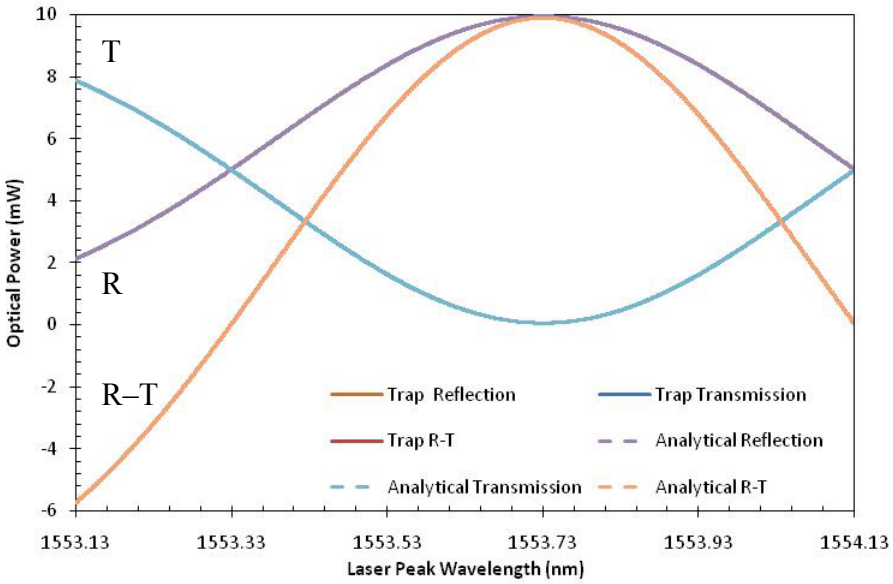

Figure 5. Output optical power from the FBG as the laser wavelength is swept across it, evaluating (7) and compared to (9) , showing the reflected optical power (R), the transmitted optical power (T), and the difference between them (R–T).

4.3 Edge Filter Detection Methods

With the successful demonstration that the numerical model could accurately reproduce the results from the analytical model, the numerical method was used with an edge filter detection method. This utilised the same light source model, but with a larger bandwidth, and greater optical power, similar to the properties of a superluminescent diode. The same sensing FBG was also utilised. In addition to this, a simple linear edge filter was used to detect the shift in the FBGs peak wavelength.

Figure 6 shows the result of linear edge filter detection. Here a 35mW superluminescent diode, with a bandwidth of 40nm (the specification of the device available for future experimental work) was used as the light source. The FBG also utilised practical values, with a reflectivity of 1, and a bandwidth of 0.8nm. These were then combined with a theoretical linear filter, which had a slope of 1, changing from a reflectivity of 0 to 1 over a span of 1nm.

In Figure 6 a) the smoothing of the relatively sharp slope (1nm wide compared to 0.8nm bandwidth of FBG) can be seen. Other than the use of a shallower filter, the model of the linear edge filter behaves as expected, giving useful results. However, if we consider a wider range of wavelength, as seen in Figure 6 b), then the bandwidth of the light source has an effect on the signal received. Effectively, this is the signal that would be generated if this light source and FBG were used in the linear edge source power detection methods.

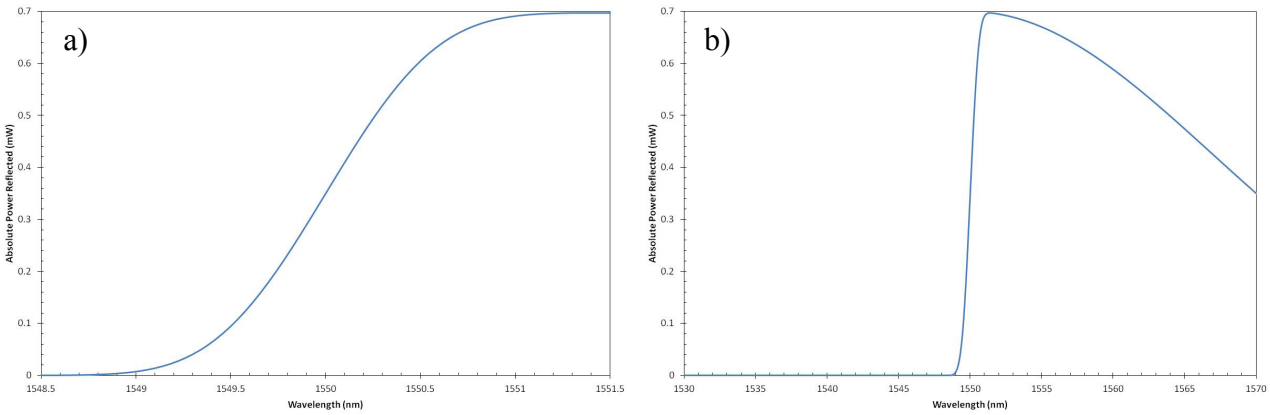

Figure 6. Response of linear edge filter detection system from the numerical solution of (11), using a light source with P=35mW, $\Delta\lambda$=40nm, an FBG with R_0=1, $\Delta\lambda_B$=0.8, and a linear edge filter with a slope of 1 from 1549.5nm to 1550.5nm.

To eliminate the issue of light source limitations, work on comparing the effect of different FBG bandwidths assumed a constant power density, of 1mW per nm. Figure 7 shows the results of varying the bandwidth of the FBG, while maintain the constant input power density (1mW per nm), and the linear edge filter with a slope of 1/nm. The bandwidth of the FBG was varied from 0.01 to 100 in quarter decade increments (4 values per decade, multiples of 1, 2.5, 5, and 7.5). The absolute received power was then divided by the maximum received power, to give the relative received power. In actuality, twice the value received at exactly 1550nm was used (which should be equal to the maximum), due to the large bandwidths at the upper end of the data being greater than the wavelength range investigate, 1530nm to 1570nm. The results clearly show that an FBG, which is significantly narrower than the linear edge filter, will accurately recover the relative slope of the filter. Conversely, an FBG that is very broad will tend to a relative slope of 0 at the midpoint of the filter. This is because as the FBG becomes much wider than the slope of the filter, the filer appears to be a step.

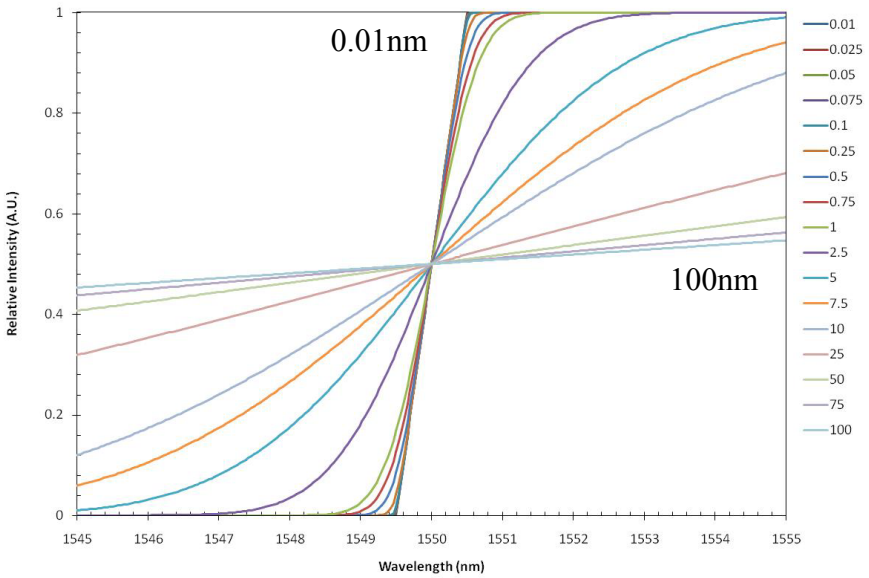

Figure 7. Effect of varying the bandwidth of the FBG on the relative reflected power, with bandwidths from 0.01nm to 100nm, with 4 points per decade.

As previously reported [5], there is once again a trade off in sensitivity (rate of change of the output, optical power, as a function of the input, Bragg wavelength) and sensing range. That is, if the sensitivity is to be a maximum, then the useful range of this filter is 1nm, its width. However, if the bandwidth of the FBG matches width of the filter, then depending on the sensitivity of the detector, the sensing range could be at most 5nm (100% interval), with a more realistic 99% (min=0.01, max=0.99) interval of 2.3nm.

Figure 8 shows the change in maximum sensitivity as a function of the FBG bandwidth. The maximum sensitivity corresponds to the slope at the midpoint of the linear edge filter, which was 1550nm. This clearly shows that the relative sensitivity is one, when the FBG bandwidth is sufficiently less than the width of the filter. Also, the relative sensitivity decays exponentially as the bandwidth of the FBG is increased.

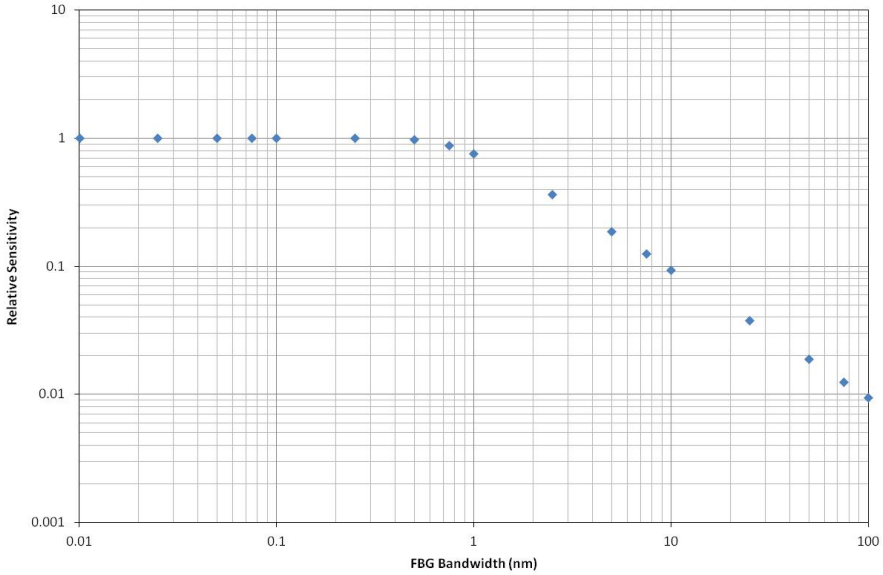

Figure 8. Change in the maximum relative sensitivity as a function of the FBG bandwidth.

5. CONCLUSION

In conclusion, we have developed a true numerical model to investigate intensity based Fibre Bragg Grating (FBG) interrogation methods. To initially test this numerical mode, it was compared with an analytical model of power detection based interrogation methods previously reported [5]. The numerical model accurately reproduced the results of the analytical model. The numerical model was then extended to incorporate edge filter based interrogation methods, which due to the complexity of the filter spectrum are not likely to give an analytical solution. As a basis to test the numerical model with an edge filter, a simple linear edge filter was used. The numerical model predicted results as expected. The numerical model enables complex relationships, in particular sensitivity to be investigated. As such, we can accurately show the change in system sensitivity of the linear edge filter interrogation method, which directly affects dynamic resolution along with signal to noise ratio.

REFERENCES

[1] Morey, W.W., Meltz, G. and Glenn, W.H. “Fiber Optic Bragg Grating Sensors,” Proc. SPIE 1169, 98–107 (1989).

[2] Meltz, G., Morey, W.W. and Glenn, W.H, “Formation of Bragg gratings in optical fibers by a transverse holographic method,” Opt. Lett. 14(15), 823–827 (1989).

[3] Kersey, A. D., "Multiplexed Bragg grating fiber sensors," Proc. LEOS '94, 153–154 (1994).
[4] Measures, R. M., [Structural monitoring with fiber optic technology], Academic Press (2001).
[5] Lee, B. and Jeong, Y., "Interrogation Techniques for Fiber Grating Sensors and the Theory of Fiber Gratings," in Fiber Optic Sensors, Yu, F. T. S. and Yin, S., Eds, Marcel Dekker, 295–381 (2002).
[6] Wild, G. and Richardson, S, "Analytical Modelling of Interrogation Systems for Fibre Bragg Grating Sensors," Proc. 35th ACOFT (2010).
[7] Nunes, L.C.S., Valente, L.C.G. and Braga, A.M.B., "Analysis of a demodulation system for fiber Bragg grating sensors using two fixed filters," Opt. Laser Eng. 42, 529–542 (2004).
[8] Othonos, A. and Kalli, K., [Fiber Bragg Gratings], Artech House (1999).
[9] Perez, I., Cui, H.L., and Udd, E., "Acoustic emission detection using fiber Bragg gratings," Proc SPIE 4328, 209–215 (2001).
[10] Cusano, A., Cutolo, A., Nasser, J., Giordano, M., and Calabrò, A., "Dynamic strain measurements by fibre Bragg grating sensor," Sensor. Actuat. A 110(1-3), 276–281 (2004).
[11] Ambrosino, C., et al., "Active vibration control using fiber Bragg grating sensors and piezoelectric actuators in co-located configuration," Proc. SPIE 6619, 661940.1- 661940.4 (2007).
[12] Fujisue, T, Nakamura, K., and Ueha, S., "Demodulation of acoustic signals in fiber Bragg grating ultrasonic sensors using arrayed waveguide gratings," Jpn. J. Appl. Phys. 45(5B), 4577–4579 (2006).
[13] Webb, D.J., et al., "Miniature fiber optic ultrasonic probe," Proc. SPIE 2839, 76–80 (1996).
[14] Takahashi, N., Hirose, A. and Takahashi, S., "Underwater acoustic sensor with fiber Bragg grating," Opt. Rev. 4(6), 691–694 (1997).
[15] Wild, G. and Hinckley, S., "A Transmit Reflect Detection System for Fibre Bragg Grating Acoustic Emission and Transmission Sensors," in Lecture Notes in Electrical Engineering - Smart Sensors and Sensing Technology, Mukhopadhyay, S. C. and Gupta, G. S., Eds., Springer, 183–197 (2008).
[16] Burden, R.L. and Faires, J. [Numerical analysis], Brooks/Cole (2001).
[17] Wild, G., Hinckley, S. and Jansz, P. V., "A transmit reflect detection system for fibre Bragg grating photonic sensors," Proc. SPIE 6801, art. no. 68010N (2007).